

Ain Shams University Faculty of Science Chemistry Department

## Corrosion behaviour of some copper alloys in LiBr solutions used in refrigeration absorption systems

Submitted to Chemistry Department
Ain Shams University
In Fulfillment of the Requirements For
The Degree of

Ph. D. in Chemistry

# By Shaimaa Esmat Abd Elhamid Abd Elaziz

M.Sc. (Chemistry), (2013)

Supervised By

Prof. Dr. S. Abdel Wahab
Prof. Dr. Ali Abd El Fattah El Warraky
Dr. Abeer Esmat El Meleigy

2020



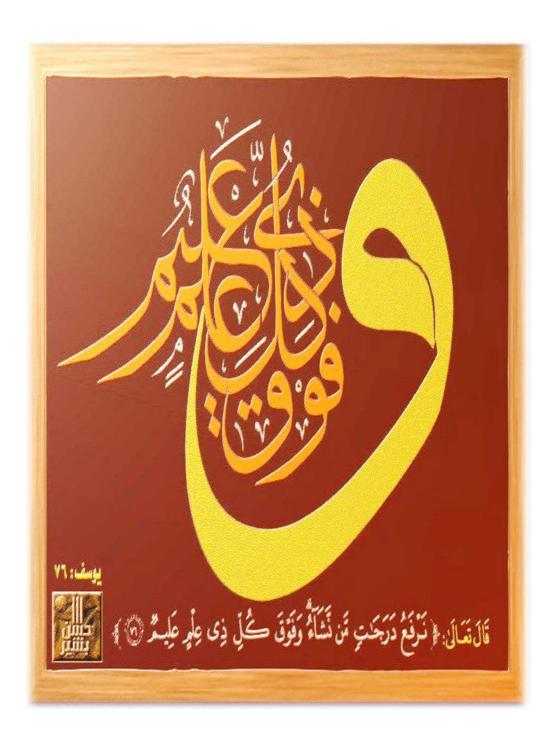
#### Ain Shams University Faculty of Science Chemistry Department

## Corrosion behaviour of some copper alloys in LiBr solutions used in refrigeration absorption systems

Thesis Approved	Thesis Advisors
Prof. Dr. S. Abdel Wahab	•••••
Prof. Dr. A. A. El Warraky	•••••
Dr. A. E. El Meleigy	

**Head of Chemistry Department** 

Prof. Dr. Ayman Ayoub Abdel-Shafi



## Acknowledgement

First, all thanks and praise are to **Allah** for giving me prosperity and strength to fulfill this work.

The author wishes to express his thanks to **Prof. Dr. S. Abdel Wahab**, professor of physical chemistry, Faculty of Science, Ain Shams University, for his interest in the work and sponsoring the thesis to the university.

Special thanks are due to **prof. Dr. A. A. El** Warraky, professor of physical chemistry department, National Research Center, Cairo for suggesting the research subject, supervision and valuable discussion.

Thanks, are also due to both **Dr. A. E. El Meleigy** and **Dr. A. Badawy**, Researcher assistance professor of physical chemistry, National Research Center, Cairo, for valuable help and assistance during the work.

The author wishes also to thank her colleges in the laboratory of electrochemistry and corrosion, National Research Center for their unfailing assistance and help.

#### **CONTENTS**

Chapter I	1
Introduction, Literature Survey and Aim of the work	1
I.1. Introduction	1
Refrigeration Absorption Systems	1
The Construction of the Chiller	2
Absorption Fluids	4
Types of Absorption Chillers	5
Advantages & Disadvantages of Absorption Chillers	6
Corrosion	7
Copper alloys	8
Aluminium bronze (Cu/7 Al)	8
Brass (Cu/30 Zn)	9
Copper Nickel	11
Pitting	12
Dealloying	14
I.2. Literature Survey	17
Corrosion problems in refrigeration absorption systems	17
Effect of some cations on the corrosion of Cu-alloys	18
The effect of corrosion product	23
Literature relating to dealloying	24
I.3. Aim of the work	28
Chapter II	30
Materials and Experimental Techniques	30
1- Material	30
i. Working electrodes	30
ii. Surface treatment of working electrodes	30
iii. Chemical and solutions	30
2- Subjects/Methods	31
2.1 Potentiodynamic Polarization Measurements	31
2.2 Current-Time Measurements	32
2.3 Surface Analysis Techniques	32
I. Scanning Electron Microscope (SEM)	32
II. Energy Dispersive X-Ray Spectroscopy (EDX)	33
2.4 Solution Analysis Measurements	35
Atomic Absorption Spectrometry (AAS)	35
Chapter III	37
Results and discussion	37
3. The Corrosion Behaviour of Cu-alloys in different concentrations of LiBr solution	is up to
9 M	37
3.1 Cyclic Potentiodynamic Polarization	37
3.2 Potentiostatic Polarization and Surface Examination	54
3.2.1 Al-bronze (Cu/7 Al)	54
3.2.2 Brass (Cu/30 Zn)	60
3.2.3 Cupronickel (Cu/10 Ni)	69
3.2.4 Cupronickel (Cu/30 Ni)	74

4. Effect of Different Types of Cations and Soluble Corrosion Product on The Dissol	lutior
of Cu/30 Ni in LiBr Solution	84
(A) Effect of Different Types of Cations	84
Cyclic Potentiodynamic Polarization in 4 M LiBr	85
1. Addition of Cu <sup>++</sup>	85
2. Addition of Ni <sup>++</sup>	87
3. Addition of Zn <sup>++</sup>	87
4. Addition of Al <sup>+++</sup>	88
Effect of Cyclic Polarization on the dissolution of Cu/30 Ni in 4 M LiBr	96
(B) Effect of Soluble Corrosion Product	99
1 Effect of Soluble Corrosion Product of Cu/30 Ni on the corrosion of Cu/30 Ni	99
2 Effect of Soluble Corrosion Product of different Cu-alloys in 4 M LiBr on the	
corrosion of Cu/30 Ni	104
2.1 Anodic Potentiodynamic Cyclic Polarization	104
2.2 Effect of Current-Time Measurement, Surface Examination and Solution An	ıalysi
	107
5. The electrochemical Behaviour of Cu/30 Ni alloy in LiBr solutions	130
5.1 Cyclic Potentiodynamic Polarization	130
5.2 Chronoamperometry and Surface Examination	131
Through I <sub>P1</sub> , at -200 mV	131
After the formation of I <sub>Max.</sub> , at +300 mV	134
After breakdown potential, at +1600 mV	136
5.3 Solution Analysis	138
6. Effect of Inhibition of Some Amino Acids on the Corrosion Behaviour of Cu/30 N	i in
LiBr Solutions	150
1- Potentiodynamic Polarization	150
2- Chronoamperometric Measurements	163
3- The Surface Analysis	171
Summary & Conclusions	182
References	194
Arabic Summary	

## LIST OF FIGURES

	Page
Fig. 1 Absorption Cycle	3
Fig. 2 Stages of Pit development	13
Fig. 3 Electrolytic cell	31
Fig. 4 Principle of EDX	34
Fig. 5 SEM, Quanta FEG 250	34
Fig. 6 Principle of Atomic Absorption spectrophotometer	36
Fig. 7 Atomic Absorption spectrophotometer	36
Fig. 8 Potentiodynamic Cyclic Polarization for Cu/7 Al in xM LiBr; (a)	$10^{-1}$ ,
(b) 1, (c) 2, (d) 4, (e) 6, (f) 9	45
Fig. 9 Potentiodynamic Cyclic Polarization for Cu/30 Zn in xM LiBr, (a)	) 10 <sup>-</sup>
<sup>1</sup> , (b) 1, (c) 2, (d) 4, (e) 6, (f) 9	46
Fig. 10 Potentiodynamic Cyclic Polarization for Cu/10 Ni in xM LiBr, (a	a) 10 <sup>-</sup>
<sup>1</sup> , (b) 1, (c) 2, (d) 4, (e) 6, (f) 9	47
Fig. 11 Potentiodynamic Cyclic Polarization for Cu $\!$ / 30 Ni in xM LiBr,	(a)
10 <sup>-1</sup> , (b) 1, (c) 2, (d) 4, (e) 6, (f) 9	48
Fig. 12 Pourbaix diagrams of pure Cu, Ni, Al and Zn (Br $\mbox{H}_{2}\mbox{O}$ system	at
25° C) in the presence of Br	49
Fig. 13 Potentiodynamic Cyclic Polarization for Cu alloys in $3x10^{-1}M$ L	.iBr,
(a) Cu/7 Al, (b) Cu/30 Zn, (c) Cu/10 Ni, (d) Cu/30 Ni	50
Fig. 14 Potentiodynamic Cyclic Polarization for Cu alloys in $5x10^{-1}~M$ L	.iBr,
(a) Cu/7 Al, (b) Cu/30 Zn, (c) Cu/10 Ni, (d) Cu/30 Ni	51
Fig. 15 Chronoamperometric curves of Cu/7 Al in $5x10^{1}\text{M}$ at different	
constant potentials (a) 300 (b) 600 mV vs SCE for 120 min.	57

Fig. 16 SEM (a) and EDX (b) of Al bronze after treated in 5x10 <sup>-1</sup> M at 300	0
mV vs SCE for 120 min.	58
Fig. 17 SEM (a) and EDX (b) of Al bronze after treated in 5x10 <sup>-1</sup> M at	<b>7</b> 0
constant potential of 600 mV vs SCE for 120 min.	59
Fig. 18 Chronoamperometric curves of Cu/30 Zn in 10 <sup>-1</sup> M at constant	
potentials of (a) 1000 and (b) 1400 mV vs SCE for 120 min.	65
Fig. 19 Chronoamperometric curves of Cu/30 Zn in 5x10 <sup>-1</sup> M at different	
constant potentials (a) 300 and (b) 900 mV vs SCE for 120 min.	66
Fig. 20 (a, b) SEM and (c) EDX of Cu/30 Zn after treated in $5x10^{-1}$ M at	
constant potentials of 300 mV vs SCE for 120 min.	67
Fig. 21 (a, b) SEM and (c, d) EDX of Cu/30 Zn after treated in $5x10^{-1}M$ a	ıt
constant potentials 900 mV vs SCE for 120 min.	68
Fig. 22 Chronoamperometric curves of Cu/10 Ni in 5x10 <sup>-1</sup> M at different	
constant potentials (a) 300 (b) 900 mV vs SCE for 120 min.	71
Fig. 23 (a, b) SEM and (c) EDX of Cu/10 Ni after treated in $5x10^{-1}$ M at	
constant potential of 300 mV vs SCE for 120 min.	72
Fig. 24 (a, b) SEM and (c) EDX of Cu/10 Ni after treated in 5x10 <sup>-1</sup> M at	
constant potential of 900 mV vs SCE for 120 min.	73

Fig. 25 Chronoamperometric curves of Cu/30 Ni in 3x10 <sup>-1</sup> M at different constant potentials (a) 150 (b) 800 (c) 1600 mV vs SCE for 120 min.	77
Fig. 26 (a, b) SEM and (c) EDX of Cu/30 Ni after treated in 3x10 <sup>-1</sup> M at constant potential of 150 mV vs SCE for 120 min.	78
Fig. 27 (a, b) SEM and (c) EDX of Cu/30 Ni after treated in $3x10^{-1}$ M at constant potential of 800 mV vs SCE for 120 min.	79
Fig. 28 (a, b) SEM and (c) EDX of Cu/30 Ni after treated in $3x10^{-1}$ M at constant potential of 1600 mV vs SCE for 120 min.	80
Fig. 29 Chronoamperometric curves of Cu/30 Ni in $5x10^{-1}$ M at constant potentials (a) 300 and (b) 900 mV vs SCE for 120 min.	81
Fig. 30 (a, b) SEM and (c) EDX of Cu/30 Ni after treated in $5x10^{-1}$ M at constant potential of 300 mV vs SCE for 120 min.	82
Fig. 31 (a, b) SEM and (c) EDX of Cu / 30 Ni after treated in $5x10^{-1}$ M at constant potential of 900 mV for 120 min.	83
Fig. 32 Potentiodynamic Cyclic Polarization for Cu/30 Ni in 4M LiBr + x ppm of Cu $^{++}$ , a (0), b (2), c (5), d (12), e (18), f (26), g (50)	90
Fig. 33 Potentiodynamic Cyclic Polarization for Cu/30 Ni in 4M LiBr + x ppm of Ni <sup>++</sup> , a (0.15), b (0.2), c (0.3), d (0.5), e (2)	91

ppm of Zn <sup>++</sup> , a (0.5), b (2)	92
Fig. 35 Potentiodynamic Cyclic Polarization for Cu/30 Ni in 4M LiBr + x ppm of $Al^{+++}$ , a (0.5), b (2)	93
Fig. 36 Potentiodynamic Cyclic Polarization for Cu $/$ 30 Ni in 4M LiBr, a (the first), b (the second), c (the third) cyclic	98
Fig. 37 Potentiodynamic Cyclic Polarization for Cu/30 Ni in xM LiBr in presence of soluble corrosion product of Cu / 30 Ni, a (2), b (4), c (6), d (9 103	))
Fig. 38 Potentiodynamic Cyclic Polarization for Cu/30 Ni in xM LiBr in presence of soluble corrosion product of Cu / 30 Ni, a (0), b (soln. Cu / 30 Ni), c (soln. Cu / 7 Al), d (soln. Cu / 10 Ni), e (soln. Cu / 30 Zn) $105$	
Fig. 39 Chronoamperometric curves of Cu/30 Ni in 4 M at different conspotentials (a) -200 (b) -300 mV 109	tant

Fig. 34 Potentiodynamic Cyclic Polarization for Cu/30 Ni in 4M LiBr + x

Fig. 40 (a, b) SEM and (c) EDX of Cu/30 Ni after treated in 4 M LiBr at

Fig. 41 (a, b) SEM and (c) EDX of Cu/30 Ni after treated in 4 M LiBr at

110

112

constant potential of -200 mV vs SCE for 120 min.

constant potential of -300 mV vs SCE for 120 min.

Fig. 42 Chronoamperometric curves of Cu/30 Ni in 4 M at constant potentials -200 mV in presence of soluble corrosion product of Cu / 30 Ni, a (0), b (soln. Cu / 30 Ni), c (soln. Cu / 10 Ni), d (soln. Cu / 7 Al), e (soln. Cu / 30 Zn), f (soln. Cu metal)

Fig. 43 (a, b, c) SEM and (d, e) EDX of Cu / 30 Ni after treated in soluble corrosion product of Cu/30 Ni in 4 M LiBr at constant potential of -200 mV vs SCE for 120 min.

Fig. 44 (a, b, c) SEM and (d, e) EDX of Cu/30 Ni after treated in soluble corrosion product of Cu/10 Ni in 4 M LiBr at constant potential of -200 mV vs SCE for 120 min.

Fig. 45 (a, b, c) SEM and (d, e) EDX of Cu/30 Ni after treated in soluble corrosion product of Cu/7 Al in 4 M LiBr at constant potential of -200 mV vs SCE for 120 min.

Fig. 46 (a, b, c) SEM and (d, e) EDX of Cu/30 Ni after treated in soluble corrosion product of Cu/30 Zn in 4 M LiBr at constant potential of -200 mV vs SCE for 120 min.

Fig. 47 (a, b, c) SEM and (d, e) EDX of Cu/30 Ni after treated in soluble corrosion product of Cu metal in 4 M LiBr at constant potential of -200 mV vs SCE for 120 min.

Fig. 48 The length of anodic passivation current ( $I_{P1}$ ) of Cu / 30 Ni in xM LiBr 142

Fig. 49 Chronoamperometric curve for Cu/30 Ni in 2 M LiBr at different applied potential (a) -200 mV (b) +300 mV (c) +1600 mV 143

Fig. 50 SEM micrograph of Cu/30 Ni electrode obtained after Chronoamperometric of Fig. 49(a) 144

Fig. 51 SEM micrograph of Cu/30 Ni electrode obtained after Chronoamperometric of Fig. 49(b) 145

Fig. 52 SEM micrograph of Cu/30 Ni electrode obtained after Chronoamperometric of Fig. 49(c) 146

Fig. 53 PCP curves of Cu/30 Ni in 6 M LiBr (a) of new sample and fresh solution and (b) new sample and the solution of experiment (a)147

Fig. 54 Potentiodynamic Cyclic Polarization for Cu/30 Ni in 2 M LiBr in the presence of different concs. of amino acids, (a) L-Lys., (b) L-Asp., (c)

Met., (d) L-Cys.

155

Fig. 55 Potentiodynamic Cyclic Polarization for Cu/30 Ni in 2 M LiBr +10<sup>-5</sup> M different concs. of amino acids with and without 10<sup>-2</sup> M KI, a (10<sup>-2</sup> M KI), b (L-Lys.), c (L-Asp.), d (L-Met.), e (L-Cys.)

Fig. 56 chronoamperometric curves for Cu/30 Ni in 2 M LiBr with 10<sup>-5</sup> and 10<sup>-2</sup> M of amino acids, (a) L-Lys, (b) L-Asp. (c), L-Met., (d) L-Cys.

165

Fig. 57 chronoamperometric curves for Cu/30 Ni in 2 M LiBr +  $10^{-5}$  M

amino acids with  $10^{-2}$  M KI, (a) L-Lys, (b) L-Asp. (c), L-Met., (d) L-Cys. 169

Fig. 58 (a) SEM and (b) EDX of Cu/30 Ni after treated in 2 M LiBr +  $10^{-5}$  M L-Lys. at a constant potential of -200 mV for 60 min. 174

Fig. 58 (c) SEM and (d) EDX of Cu/30 Ni after treated in 2 M LiBr +  $10^{-5}$  M L-Lys. +  $10^{-2}$  M KI at a constant potential of -200 mV for 60 min. 175

Fig. 59 (a) SEM and (b) EDX of Cu/30 Ni after treated in 2 M LiBr  $+ 10^{-5}$  M L-Asp. at a constant potential of -200 mV for 60 min. 176

Fig. 59 (c) SEM and (d) EDX of Cu/30 Ni after treated in 2 M LiBr +  $10^{-5}$  M L-Asp. +  $10^{-2}$  M KI at a constant potential of -200 mV for 60 min. 177

Fig. 60 (a) SEM and (b) EDX of Cu/30 Ni after treated in 2 M LiBr + 10<sup>-5</sup> M L-Met. at constant potential of -200 mV for 60 min.

Fig. 60 (c) SEM and (d) EDX of Cu/30 Ni after treated in 2 M LiBr +  $10^{-5}$  M L-Met. +  $10^{-2}$  M KI at constant potential of -200 mV for 60 min.179

Fig. 61 (a) SEM and (b) EDX of Cu/30 Ni after treated in 2 M LiBr  $+ 10^{-5}$  M L-Cys. at a constant potential of -200 mV for 60 min. 180

Fig. 61 (a) SEM and (b) EDX of Cu/30 Ni after treated in 2 M LiBr +  $10^{-5}$  M L-Cys. +  $10^{-2}$  M KI at a constant potential of -200 mV for 60 min. 181

### LIST OF TABLES

Pa	ge
Table 1 The requirements for the refrigerant and an absorbent material in the refrigeration system 3	
Table 2 Types of Absorption Chillers 5	
Table 3 Properties of Brasses	0
Table 4 Corrosion potential ( $E_{Corr.}$ ), corrosion current densities ( $I_{Corr.}$ ), anodicurrent maximum ( $I_{Max.}$ ), the breakdown potential after passivation current ( $E_{break}$ ), the protection potential ( $E_{Prot}$ ), the hysteresis loop length ( $E_{break.} - E_{Prot}$ ), the length of the passive region ( $E_{break} - E_{Corr}$ ), these parameters are for bot $Cu/7$ Al and $Cu/30$ Zn alloys	nt rot th
Table 5 Corrosion potential ( $E_{Corr.}$ ), corrosion current densities ( $I_{Corr.}$ ), anodicurrent maximum ( $I_{Max.}$ ), the breakdown potential after passivation current ( $E_{break}$ ), the protection potential ( $E_{Prot}$ ), the hysteresis loop length ( $E_{break}E_{Prot}$ ) the length of the passive region ( $E_{break}-E_{Corr.}$ ), these parameter are for both Cu /10 Ni and Cu /30 Ni alloys	nt rot th
Table 6 Atomic absorption analysis of Cu, Zn and their ratios for Cu/30 Zn i 5x10 <sup>-1</sup> M LiBr	

Table 7 Corrosion potential ( $E_{Corr.}$ ), anodic current maximum ( $I_{Max.}$ ) for Cu/30 Ni in 4 M LiBr without and with different concentration of  $Cu^{++}$  94

Table 8 Corrosion potential ( $E_{Corr.}$ ), anodic current maximum ( $I_{Max.}$ ) for Cu/30 Ni in 4 M LiBr without and with different concentration of Ni<sup>++</sup> 94

Table 9 Corrosion potential ( $E_{Corr.}$ ), anodic current maximum ( $I_{Max.}$ ) for Cu/30 Ni in 4 M LiBr without and with different concentration of  $Zn^{++}$  95

Table 10 Corrosion potential ( $E_{Corr.}$ ), anodic current maximum ( $I_{Max.}$ ) for Cu/30 Ni in 4 M LiBr without and with different concentration of Al<sup>+++</sup> 95

Table 11 Corrosion potential ( $E_{Corr.}$ ), anodic current maximum ( $I_{Max.}$ ), the first and the second peak potential  $E_{P1}$  and  $E_{P2}$ , the first and the second peak current density  $I_{P1}$  and  $I_{P2}$ , the breakdown potential ( $E_{break}$ ), the breakdown current density ( $I_{break.}$ ) the protection potential ( $E_{Prot.}$ ), the protection current density ( $I_{Prot.}$ ) the hysteresis loop length ( $E_{break.} - E_{Prot}$ ) for Cu/30 Ni in solution of 4 M LiBr for the first, the second and the third cycle

Table 12 Corrosion potential ( $E_{Corr.}$ ), anodic current maximum ( $I_{Max.}$ ), the first peak potential  $E_{P1}$ , the first peak current density  $I_{P1}$  and  $I_{P2}$ , the breakdown potential ( $E_{break}$ ), the breakdown current density ( $I_{break.}$ ) the protection potential ( $E_{Prot.}$ ), the protection current density ( $I_{Prot.}$ ) the hysteresis loop length ( $E_{break.} - E_{Prot.}$ ) for Cu/30 Ni in different concentrations of LiBr solutions with soluble corrosion product

Table 13 Corrosion potential (E<sub>Corr.</sub>), anodic current maximum (I<sub>Max.</sub>), the